Implementation and verification of a hyper-viscoelastic constitutive model in Abaqus/Explicit

Ruben Løland Sælen

July 2023

1 Introduction

This document serves as an overview of the material model I implemented to describe a photopolymer resin as part of my PhD. The description of the model is kept brief and the reader is referred to my thesis for a more detailed description.

2 Model formulation

2.1 Overview

The model consists of a hyperelastic spring (Part A) in parallel with a hyper-viscoelastic network (Part B) and is illustrated in Figure 1. Both Part A and Part B are governed by the total deformation gradient, viz.

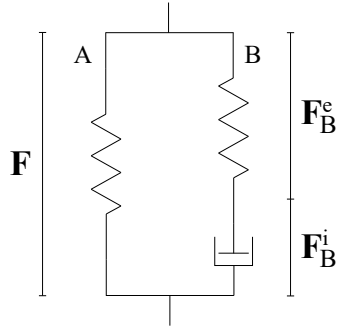$$\mathbf{F} = \mathbf{F}_A = \mathbf{F}_B \tag{1}$$

Figure 1: Rheological model.

The deformation gradient of Part B is multiplicatively decomposed into an elastic part, $\mathbf{F}_B^e$, and an

inelastic part, $\mathbf{F}_{\mathrm{B}}^{\mathrm{i}}$, by the use of an intermediate configuration, viz.

$$\mathbf{F}_{\mathrm{B}} = \mathbf{F}_{\mathrm{B}}^{\mathrm{e}}\mathbf{F}_{\mathrm{B}}^{\mathrm{i}} \tag{2}$$

The Helmholtz free energy function per unit volume of the model is additively composed as

$$\psi = \psi_{\mathrm{A}} + \psi_{\mathrm{B}} \tag{3}$$

which also results in an additive decomposition of the Cauchy stress tensor

$$\boldsymbol{\sigma} = \boldsymbol{\sigma}_{\mathrm{A}} + \boldsymbol{\sigma}_{\mathrm{B}} \tag{4}$$
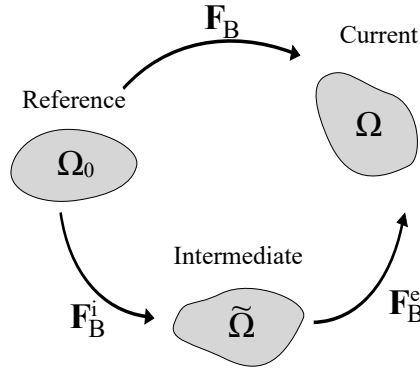

Figure 2: The kinematics of Part B.

2.2 Part A

The Cauchy stress of Part A is defined by the Arruda-Boyce model [1] as

$$\boldsymbol{\sigma}_{\mathrm{A}} = \frac{\mu_{\mathrm{A}}\lambda_{\mathrm{L}}}{3\bar{\lambda}_{\mathrm{c}}J}\mathcal{L}^{-1}\left(\frac{\bar{\lambda}_{\mathrm{c}}}{\lambda_{\mathrm{L}}}\right)\bar{\mathbf{B}}' \tag{5}$$

where μ_{A} and λ_{L} are the initial shear modulus and locking stretch of Part A respectively. $\bar{\mathbf{B}}'$ is the deviatoric part of the isochoric left Cauchy-Green deformation tensor, $\bar{\mathbf{B}} = J^{-2/3}\mathbf{F}\mathbf{F}^{\mathrm{T}}$. The effective chain stretch $\bar{\lambda}_{\mathrm{c}}$ is defined as $\bar{\lambda}_{\mathrm{c}} = \sqrt{\mathrm{tr}(\bar{\mathbf{B}})/3}$, where $\mathrm{tr}(\bar{\mathbf{B}}) = \bar{B}_{kk}$. The Langevin function is defined as $\mathcal{L}(x) = \coth x - 1/x$.

The hyperelastic element exhibits an initial linear response followed by a rapid increase in stress level as the value of the effective chain stretch approaches the locking stretch.

2.3 Part B

The Cauchy stress of the hyperelastic element in Part B is defined by the neo-Hookean model as

2

$$\boldsymbol{\sigma}_{\mathrm{B}} = \frac{\mu_{\mathrm{B}}}{J}\bar{\mathbf{B}}_{\mathrm{B}}^{\mathrm{e}'} + \kappa(J-1)\mathbf{I} \tag{6}$$

where $\bar{\mathbf{B}}_{\mathrm{B}}^{\mathrm{e}'}$ is the deviatoric part of the elastic isochoric left Cauchy-Green deformation tensor, $\bar{\mathbf{B}}_{\mathrm{B}}^{\mathrm{e}} = J^{-2/3}\mathbf{F}_{\mathrm{B}}^{\mathrm{e}}(\mathbf{F}_{\mathrm{B}}^{\mathrm{e}})^{\mathrm{T}}$, $\mathbf{I}$ is the second-order identity tensor, μ_{B} is the shear modulus of Part B and κ is the bulk modulus.

By the multiplicative split of the deformation gradient, the total velocity gradient of Part B is additively decomposed into an elastic part and inelastic part as

$$\mathbf{L}_{\mathrm{B}} = \dot{\mathbf{F}}_{\mathrm{B}}^{\mathrm{e}}(\mathbf{F}_{\mathrm{B}}^{\mathrm{e}})^{-1} + \mathbf{F}_{\mathrm{B}}^{\mathrm{e}}\dot{\mathbf{F}}_{\mathrm{B}}^{\mathrm{i}}(\mathbf{F}_{\mathrm{B}})^{-1} = \mathbf{L}_{\mathrm{B}}^{\mathrm{e}} + \mathbf{L}_{\mathrm{B}}^{\mathrm{i}} \tag{7}$$

where $\mathbf{L}_{\mathrm{B}}^{\mathrm{i}} = \mathbf{D}_{\mathrm{B}}^{\mathrm{i}} + \mathbf{W}_{\mathrm{B}}^{\mathrm{i}}$. Both the inelastic rate of deformation tensor, $\mathbf{D}_{\mathrm{B}}^{\mathrm{i}}$, and inelastic spin tensor, $\mathbf{W}_{\mathrm{B}}^{\mathrm{i}}$, need to be prescribed for a unique solution to be attainable. Due to isotropy, the inelastic spin tensor is taken as $\mathbf{W}_{\mathrm{B}}^{\mathrm{i}} = \mathbf{0}$ [2, 3]. The inelastic rate of deformation tensor is described by a flow rule on the form

$$\mathbf{D}_{\mathrm{B}}^{\mathrm{i}} = \dot{\gamma}_{\mathrm{B}}\frac{3}{2}\frac{\boldsymbol{\sigma}_{\mathrm{B}}'}{\sigma_{\mathrm{vm,B}}} \tag{8}$$

where $\dot{\gamma}_{\mathrm{B}}$ is an effective inelastic strain rate, $\boldsymbol{\sigma}_{\mathrm{B}}'$ is the deviatoric part of the Cauchy stress tensor in Part B and the equivalent von Mises stress of Part B is defined as $\sigma_{\mathrm{vm,B}} = \sqrt{3/2\boldsymbol{\sigma}_{\mathrm{B}}' : \boldsymbol{\sigma}_{\mathrm{B}}'}$. Note that since $\mathbf{D}_{\mathrm{B}}^{\mathrm{i}}$ is deviatoric, no volume change due to inelastic deformation occurs. This can be seen from the expression for the rate of change of the inelastic Jacobian determinant, $\dot{J}_{\mathrm{B}}^{\mathrm{i}} = J_{\mathrm{B}}^{\mathrm{i}}\mathrm{tr}(\mathbf{D}_{\mathrm{B}}^{\mathrm{i}})$, where the trace of the inelastic rate of deformation tensor is zero and consequently $\dot{J}_{\mathrm{B}}^{\mathrm{i}} = 0$.

The effective inelastic strain rate $\dot{\gamma}_{\mathrm{B}}$ also needs to be prescribed. A modified version of the viscoelastic constitutive relation proposed by Bergström and Boyce [4] is used in this model. The expression reads

$$\dot{\gamma}_{\mathrm{B}} = \dot{\gamma}_0\left(\frac{\sigma_{\mathrm{vm,B}}}{\bar{\tau}}\right)^m \tag{9}$$

where $\dot{\gamma}_0$ is a reference strain rate, m is a material constant and $\bar{\tau}$ is the effective shear resistance to viscous flow. Note that the deformation dependence on viscous flow from the Bergström-Boyce model is omitted.

The effective shear resistance is taken to depend on hydrostatic stress as

$$\bar{\tau} = \tau - \alpha\sigma_{\mathrm{H,B}} > 0 \tag{10}$$

where $\sigma_{\mathrm{H,B}} = \mathrm{tr}(\boldsymbol{\sigma}_{\mathrm{B}})/3$ and α is a pressure sensitivity parameter. Strain softening is captured through the phenomenological evolution of the shear resistance τ proposed by Boyce et al. [5]

3

$$\dot{\tau} = h\left(1 - \frac{\tau}{\tau_{\mathrm{ss}}}\right)\dot{\gamma}_{\mathrm{B}} \tag{11}$$

where h is a softening parameter and τ_{ss} is the saturation value of τ. The initial value of τ is the parameter τ_0.

The material parameters of the hyper-viscoelastic model are summarised in Table 1.

Table 1: Hyper-viscoelastic material parameters.

Parameter	Unit	Description
μ_{A}	MPa	Shear modulus Part A
μ_{B}	MPa	Shear modulus Part B
λ_{L}	-	Locking stretch
κ	MPa	Bulk modulus
$\dot{\gamma}_0$	s^{-1}	Reference strain rate
m	-	Strain-rate sensitivity parameter
h	MPa	Softening modulus
τ_0	MPa	Initial shear strength
τ_{ss}	MPa	Saturated shear strength
α	-	Pressure sensitivity parameter

2.4 Fracture model

A stochastic fracture model is adapted from Holmström et al. [6]. Fracture occurs when an equivalent stress, $\bar{\sigma}$, reaches a critical stress level, $\bar{\sigma}_{\mathrm{c}}$. The equivalent stress is defined as

$$\bar{\sigma} = \sqrt{\sum_{I=1}^{3} \langle \sigma_I \rangle^2} \tag{12}$$

where $\langle \cdot \rangle$ is the positive Macaulay bracket and the principal stresses of the Cauchy stress tensor, σ_I, are ordered as $\sigma_1 \geq \sigma_2 \geq \sigma_3$. An equivalent strain measure, $\bar{\varepsilon}$, is defined to be power conjugate with the equivalent stress. Equivalence in mechanical power gives

$$\bar{\sigma}\dot{\bar{\varepsilon}} = \boldsymbol{\sigma} : \mathbf{D} \rightarrow \bar{\varepsilon} = \int_0^t \frac{1}{\bar{\sigma}} \boldsymbol{\sigma} : \mathbf{D} \mathrm{d}t \tag{13}$$

where $\mathbf{D}$ is the total rate of deformation tensor, $\mathbf{D} = (\mathbf{L} + \mathbf{L}^{\mathrm{T}})/2$, and $\mathbf{L}$ is the total velocity gradient, $\mathbf{L} = \dot{\mathbf{F}}\mathbf{F}^{-1}$.

The crack-band model [7] is used to regularise the fracture by intorucing the fracture energy parameter, G_{f}. The procedure is illustrated in Figure 3 where G_{f} is seen to represent the shaded area of the curve, i.e., the energy dissipated at fracture. When the critical equivalent stress is reached, linear strain softening takes place until the equivalent failure strain, $\bar{\varepsilon}_{\mathrm{u}}$, is reached. An expression
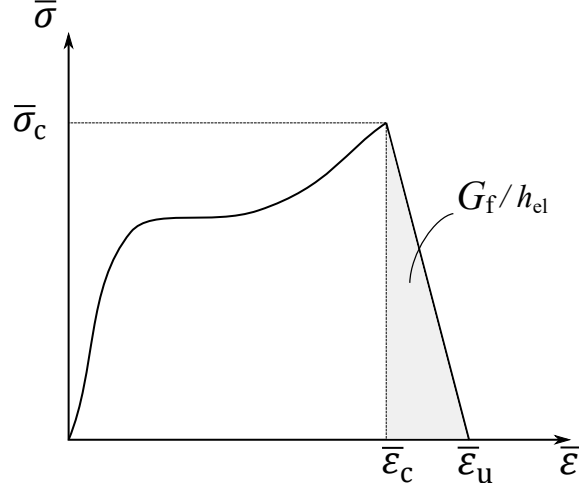
4

Figure 3: Equivalent stress vs equivalent strain curve showing how G_f is related to the dissipated energy at fracture.

for $\bar{\varepsilon}_u$ is obtained by equating the fracture energy of the crack surface with the dissipated strain energy of the element

$$G_f A_{el} = \frac{1}{2}\bar{\sigma}_c(\bar{\varepsilon}_u - \bar{\varepsilon}_c)V_{el} \tag{14}$$

where A_{el} is the area of the crack surface, V_{el} is the volume of the element and $\bar{\varepsilon}_c$ is the equivalent strain corresponding to the critical stress $\bar{\sigma}_c$. By assuming cubic elements with a characteristic size h_{el}, the equivalent failure strain is found as

$$\bar{\varepsilon}_u = \bar{\varepsilon}_c + \frac{2G_f}{\bar{\sigma}_c h_{el}} \tag{15}$$

It is emphasised that the fracture energy parameter, G_f, is not related to the material behaviour and is strictly a numerical parameter.

To prevent spurious element erosion due to stress waves, the equivalent stress needs to be equal to or greater than the critical stress during a defined critical time interval, Δt_c.

In the softening stage, the stress tensor in the constitutive equations is replaced by an effective stress tensor defined as

$$\boldsymbol{\sigma}_{\text{eff}} = \frac{\boldsymbol{\sigma}}{(1-\delta)} \tag{16}$$

where δ is a damage variable defined as

$$\delta = \begin{cases} 0 & \text{for } \bar{\varepsilon} < \bar{\varepsilon}_{\mathrm{c}} \\ 1 - \dfrac{\bar{\varepsilon}_{\mathrm{u}} - \bar{\varepsilon}}{\bar{\varepsilon}_{\mathrm{u}} - \bar{\varepsilon}_{\mathrm{c}}} & \text{for } \bar{\varepsilon} \geq \bar{\varepsilon}_{\mathrm{c}} \end{cases} \tag{17}$$

Stochastic fracture is introduced by making the critical equivalent stress, $\bar{\sigma}_{\mathrm{c}}$, follow a left-truncated normal distribution. The probability density function of $\bar{\sigma}_{\mathrm{c}}$ is given as

$$f(\bar{\sigma}_{\mathrm{c}}) = \frac{1}{\bar{\sigma}_{\mathrm{c,std}}\sqrt{2\pi}} \exp\left[-\frac{1}{2}\left(\frac{\bar{\sigma}_{\mathrm{c}} - \bar{\sigma}_{\mathrm{c,mean}}}{\bar{\sigma}_{\mathrm{c,std}}} \right)^2 \right] \tag{18}$$

and is made left-truncated through the definition

$$f_{\mathrm{LT}}(\bar{\sigma}_{\mathrm{c}}) = \begin{cases} 0 & \text{for } \bar{\sigma}_{\mathrm{c}} < \bar{\sigma}_{\mathrm{c,min}} \\ \dfrac{f(\bar{\sigma}_{\mathrm{c}})}{\int_{\bar{\sigma}_{\mathrm{c,min}}}^{\infty} f(\bar{\sigma}_{\mathrm{c}})\mathrm{d}\bar{\sigma}_{\mathrm{c}}} & \text{for } \bar{\sigma}_{\mathrm{c}} \geq \bar{\sigma}_{\mathrm{c,min}} \end{cases} \tag{19}$$

The stochastic failure stress is distributed to the material points of a finite element model through an assignment mesh, as proposed by Knoll [8]. The assignment mesh has the shape of a rectangular cuboid and covers the entire finite element model. A random critical stress according to the distribution in Eq. 19 is assigned to each element in the assignment mesh. Each integration point in the finite element model that lies inside an element of the assignment mesh is then assigned the critical stress value of the assignment element. It is apparent that the element size of the assignment mesh controls the length scale of $\bar{\sigma}_{\mathrm{c}}$. Figure 4 (a) shows the critical stress distribution in a finite element model of a tensile test assigned with an assignment element size twice as large as the finite element size in the gauge area. Figure 4 (b) shows a histogram of the fracture stresses together with the nominal distribution used to generate the random variables.
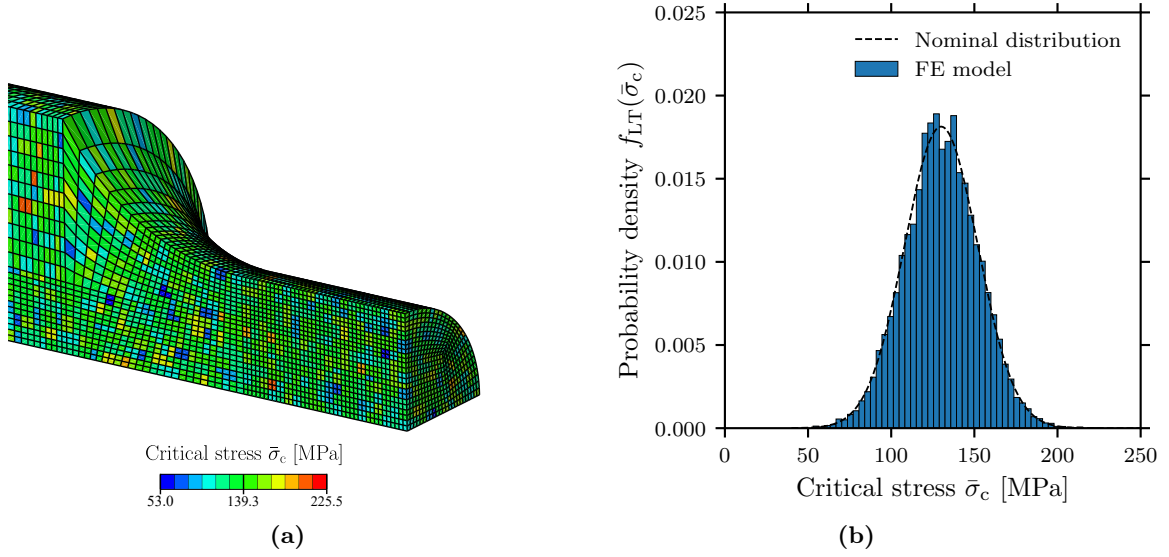
Figure 4: (a) Critical stress distribution in the gauge area of a FE model of a smooth tensile specimen and (b) a comparison between the nominal distribution and the distribution in the FE model with a normalised histogram.

The parameters used in the fracture model are summarised in Table 2.

Table 2: Fracture model parameters.

Parameter	Unit	Description
$\bar{\sigma}_{c,mean}$	MPa	Mean value of the stochastic failure stress
$\bar{\sigma}_{c,std}$	MPa	Standard deviation of the stochastic failure stress
$\bar{\sigma}_{c,min}$	MPa	Minimum value of the stochastic failure stress
G_f	N/mm	Fracture energy release parameter
Δt_c	s	Critical time interval

3 Numerical implementation

The constitutive model is implemented in Abaqus/Explicit. A quasi-implicit numerical integration scheme inspired by Johnsen et al. [9] was used to integrate the flow rule in Eq. 8. Inserting the relation between the inelastic deformation gradient and the inelastic rate of deformation tensor into the equation gives

$$\dot{\mathbf{F}}^i_B = \dot{\gamma}_B (\mathbf{F}^e_B)^{-1} \mathbf{N}^i_B \mathbf{F}^e_B \mathbf{F}^i_B \tag{20}$$

which can be solved with a backward Euler approximation as

7

$$\mathbf{F}^{\mathrm{i}}_{\mathrm{B},n+1} = \mathbf{F}^{\mathrm{i}}_{\mathrm{B},n} + (\dot{\gamma}_{\mathrm{B}}(\mathbf{F}^{\mathrm{e}}_{\mathrm{B}})^{-1}\mathbf{N}^{\mathrm{i}}_{\mathrm{B}}\mathbf{F})\big|_{n+1}\Delta t_{n+1} \tag{21}$$

The above equation may be rearranged and solved iteratively as

$$(\mathbf{F}^{\mathrm{i},I}_{\mathrm{B},n+1})^{-1} = (\mathbf{I} - \dot{\gamma}^{I}_{\mathrm{B},n+1}\Delta t_{n+1}\mathbf{F}^{-1}_{n+1}\mathbf{N}^{\mathrm{i},I-1}_{\mathrm{B},n+1}\mathbf{F}_{n+1})(\mathbf{F}^{\mathrm{i}}_{\mathrm{B},n})^{-1} \tag{22}$$

where the superscript I signifies the Ith iteration. Note that in order to avoid equation solving, the direction of inelastic flow, $\mathbf{N}^{\mathrm{i}}_{\mathrm{B}}$, lags one iteration behind the other iterative variables. With the inverse inelastic deformation gradient at hand, the elastic part is calculated as

$$\mathbf{F}^{\mathrm{e},I}_{\mathrm{B},n+1} = \mathbf{F}_{n+1}\left(\mathbf{F}^{\mathrm{i},I}_{\mathrm{B},n+1}\right)^{-1} \tag{23}$$

which is used in the calculation of the Cauchy stress tensor $\boldsymbol{\sigma}^{I}_{\mathrm{B,n+1}}$.

The effective inelastic strain rate of the next iteration is calculated using the secant method

$$\dot{\gamma}^{I+1}_{\mathrm{B},n+1} = \dot{\gamma}^{I}_{\mathrm{B},n+1} - \frac{\dot{\gamma}^{I}_{\mathrm{B},n+1} - \dot{\gamma}^{I-1}_{\mathrm{B},n+1}}{r^{I}_{n+1} - r^{I-1}_{n+1}}r^{I}_{n+1} \tag{24}$$

where r^{I}_{n+1} is a residual function defined as

$$r^{I}_{n+1} = \dot{\gamma}^{I}_{\mathrm{B},n+1} - \dot{\gamma}_0\left(\frac{\sigma^{I}_{\mathrm{vm,B,n+1}}}{\bar{\tau}^{I}_{n+1}}\right)^{m} \tag{25}$$

To start the iteration, values for $\dot{\gamma}^{0}_{\mathrm{B},n+1}$ and $\dot{\gamma}^{1}_{\mathrm{B},n+1}$ are needed. For the first time step, $\dot{\gamma}^{1}_{\mathrm{B},1}$ is taken to be close to zero while $\dot{\gamma}^{0}_{\mathrm{B},1} = 0$. For the remaining time steps, the initial guesses are $\dot{\gamma}^{0}_{\mathrm{B},n+1} = \dot{\gamma}_{\mathrm{B},n}$ and $\dot{\gamma}^{1}_{\mathrm{B},n+1} = \dot{\gamma}_0\left(\frac{\sigma^{0}_{\mathrm{vm,B,n+1}}}{\bar{\tau}^{0}_{n+1}}\right)^{m}$ [10]. Iterations are performed until the absolute value of the residual defined in Eq. 25 is less than a defined tolerance.

The evolution of the effective shear strength is solved fully implicitly with the backward Euler method as

$$\tau^{I+1}_{n+1} = \frac{\tau_n + h\dot{\gamma}^{I+1}_{\mathrm{B},n+1}\Delta t_{n+1}}{1 + \dfrac{h}{\tau_{\mathrm{ss}}}\dot{\gamma}^{I+1}_{\mathrm{B},n+1}\Delta t_{n+1}} \tag{26}$$

When the material routine has converged and the Cauchy stress tensor for the current time step has been obtained, the damage variable, δ_{n+1}, is calculated in accordance with Eq. 17. The stress tensor returned to Abaqus/Explicit at the end of the VUMAT has to be oriented in the reference configuration such that the FE solver can calculate the appropriate objective stress rate. The hyperelastic relations in the presented material model are calculated using the left Cauchy-Green

deformation tensor, and the stress tensors are thus oriented in the current configuration. The irrotational Cauchy stress tensor returned to Abaqus at the end of the material routine is

$$\hat{\boldsymbol{\sigma}}_{n+1} = (\mathbf{R}_{n+1})^{\mathrm{T}} \boldsymbol{\sigma}_{\mathrm{eff},n+1} \mathbf{R}_{n+1} (1 - \delta_{n+1}) \tag{27}$$

where $\mathbf{R}_{n+1}$ is the rotation tensor calculated as $\mathbf{R}_{n+1} = \mathbf{F}_{n+1} \mathbf{U}_{n+1}^{-1}$. The right stretch tensor at the current time step, $\mathbf{U}_{n+1}$, is provided by the Abaqus VUMAT interface.

As the time evolution of the inelastic deformation gradient in Eq. 20 is integrated with a first-order approximation, situations may arise where the strain increment provided by the Abaqus VUMAT interface, $\Delta\boldsymbol{\varepsilon}$, is too large for convergence to be achieved. A sub-stepping scheme is introduced to improve the robustness of the model for these cases. The number of sub-steps performed, N_{sub}, is determined by the following expression

$$N_{\mathrm{sub}} = \max\left\{ \mathrm{nint}\left[\frac{\Delta\varepsilon_{\mathrm{eq}}}{\Delta\varepsilon_{\mathrm{cr}}} \right], 1 \right\} \tag{28}$$

where $\mathrm{nint}[\cdot]$ is the nearest-integer function, $\Delta\varepsilon_{\mathrm{eq}}$ is the equivalent deviatoric strain increment calculated as $\Delta\varepsilon_{\mathrm{eq}} = \sqrt{\frac{2}{3}\Delta\boldsymbol{\varepsilon}' : \Delta\boldsymbol{\varepsilon}'}$, $\Delta\boldsymbol{\varepsilon}'$ is the deviatoric part of the strain increment tensor and $\Delta\varepsilon_{\mathrm{cr}}$ is a critical strain increment. The critical strain increment is calculated based on the initial shear strength and shear modulus of Part B as

$$\Delta\varepsilon_{\mathrm{cr}} = \chi \frac{\tau_0}{\mu_{\mathrm{B}}} \tag{29}$$

where χ is a numerical parameter that determines the magnitude of the critical strain increment. Unless otherwise stated, a value of 10^{-4} is used for χ for the remainder of this work.

During sub-stepping, the current total deformation gradient, $\mathbf{F}_{n+1}$, in the above expressions is replaced with the total deformation gradient evaluated at time $t_{n+\theta}$ defined as

$$\mathbf{F}_{n+\theta} = \theta\mathbf{F}_{n+1} + (1 - \theta)\mathbf{F}_n \tag{30}$$

where

$$\theta = \frac{q}{N_{\mathrm{sub}}} \quad \text{for} \quad q \in [0, N_{\mathrm{sub}}] \tag{31}$$

Normal-distributed variables in accordance with Eq. 19 were generated with the Marsaglia polar method [11] and the left truncation was enforced by rejection sampling.

4 Verification

The implementation of the material model is verified by conducting single-element simulations. A C3D8R element with dimensions $1 \times 1 \times 1$ mm^3 was used for all simulations. Appropriate boundary conditions were applied to achieve the desired stress states and the prescribed deformation was achieved by prescribing nodal velocities. Mass scaling was used to reduce the computational time of the simulations. The element used in the uniaxial tension simulations is shown as an example in Figure 5.
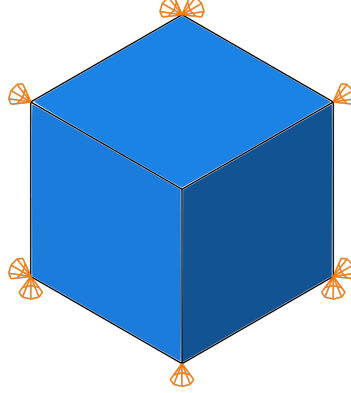
Figure 5: Finite element with boundary conditions corresponding to uniaxial tension and compression.

Single-element simulations were carried out where one material parameter was varied while the other parameters were assigned the values in Table 3. The results from the single-element simulations studying the effects of the hyper-viscoelastic material parameters are shown in Figure 6, 7, 8 and 9. The main findings are summarised as:

- **The shear modulus of Part A,** μ_A, determines the slope of the Part A stress. The effect is most noticeable during inelastic flow when the stress from Part B is no longer increasing.

- **The locking stretch,** λ_L, determines the vertical asymptote of the stress-strain curve. It also has a slight effect on the slope of the Part A stress, in accordance with Eq. 5.

- **The shear modulus of Part B,** μ_B, determines the slope of the initial elastic region of the stress-strain curve.

- **The initial shear strength**, τ_0, determines the flow stress of the material. When the saturated shear strength remains unchanged, the stress-strain curves for the different values of τ_0 converge rather quickly after the inelastic flow occurs.

- **The saturated shear strength**, τ_ss, determines the drop in stress after yield due to strain softening.

- **The softening modulus**, h, determines the rate of the strain softening.

- **The strain-rate sensitivity parameter**, m, determines both the strain-rate sensitivity of the flow stress as well as the shape of the stress-strain curve in the transition from pure elasticity to inelastic flow. The last point is seen clearly in Figure 8 (b).

- **The pressure sensitivity parameter**, α, determines the difference in flow stress between uniaxial tension and uniaxial compression. Unlike most pressure-sensitive plasticity models, the pressure sensitivity parameter in the implemented model affects the flow stress in tension.

Table 3: Material parameters used in the verification simulations.

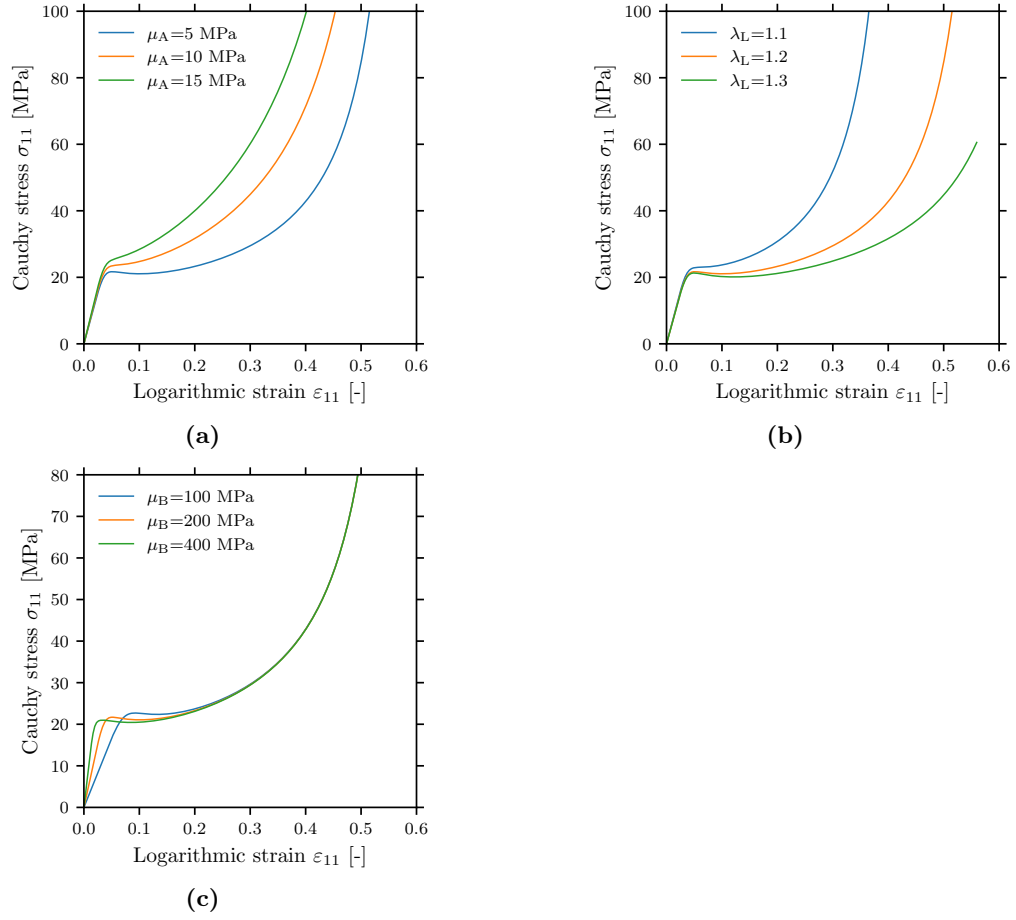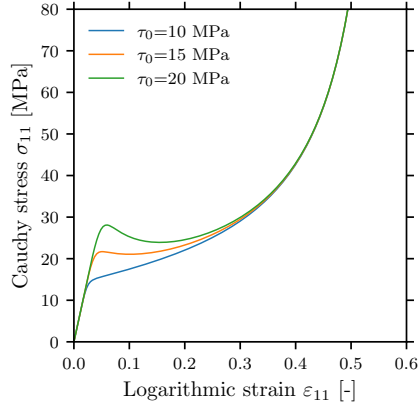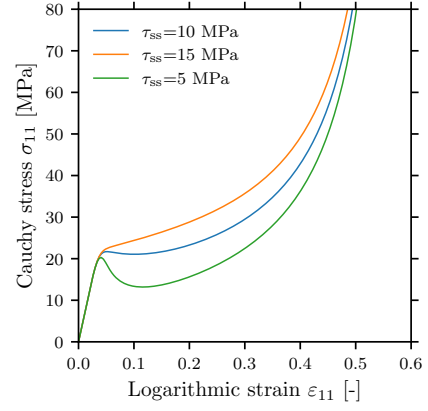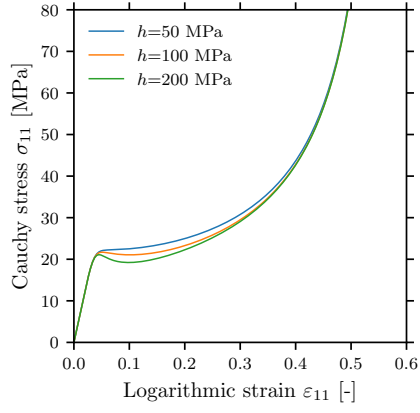| Part A	μ_{A} [MPa]	λ_{L} [-]						
	5	1.2						
Part B	μ_{B} [MPa]	κ [MPa]	$\dot{\gamma}_0$ [s^{-1}]	m [-]	τ_0 [MPa]	τ_{ss} [MPa]	h [MPa]	α [-]
	200	2000	10^{-3}	6	15	10	100	0.1

(a)

(b)

(c)

Figure 6: Stress vs. strain curves from uniaxial tension single element simulations at a nominal strain rate of $10^{-2}\,\mathrm{s}^{-1}$. The effects of μ_{A}, λ_{L} and μ_{B} on the stress-strain response are shown in **(a)**, **(b)** and **(c)** respectively.

(a)

(b)

(c)

Figure 7: Stress vs. strain curves from uniaxial tension single element simulations at a nominal strain rate of $10^{-2}\,\mathrm{s}^{-1}$. The effects of τ_0, τ_{ss} and h on the stress-strain response are shown in **(a)**, **(b)** and **(c)** respectively.

(a) $\dot{e} = 10^{-3}$ s^{-1}

(b) $\dot{e} = 10^{-3}$ s^{-1} – Zoomed-in

(c) $\dot{e} = 10^{-2}$ s^{-1}

(d) $\dot{e} = 10^{-1}$ s^{-1}
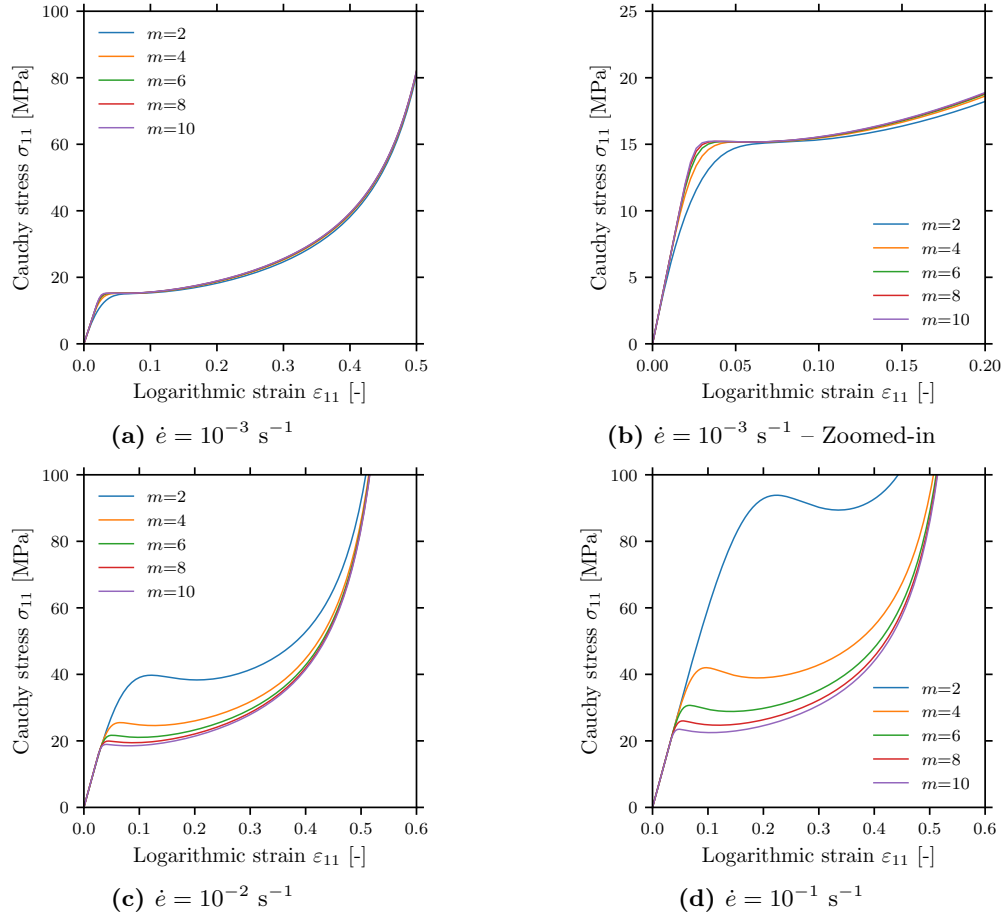
Figure 8: Stress vs. strain curves from uniaxial tension single element simulations showing how the parameter m affects the stress-strain response at different nominal strain rates.
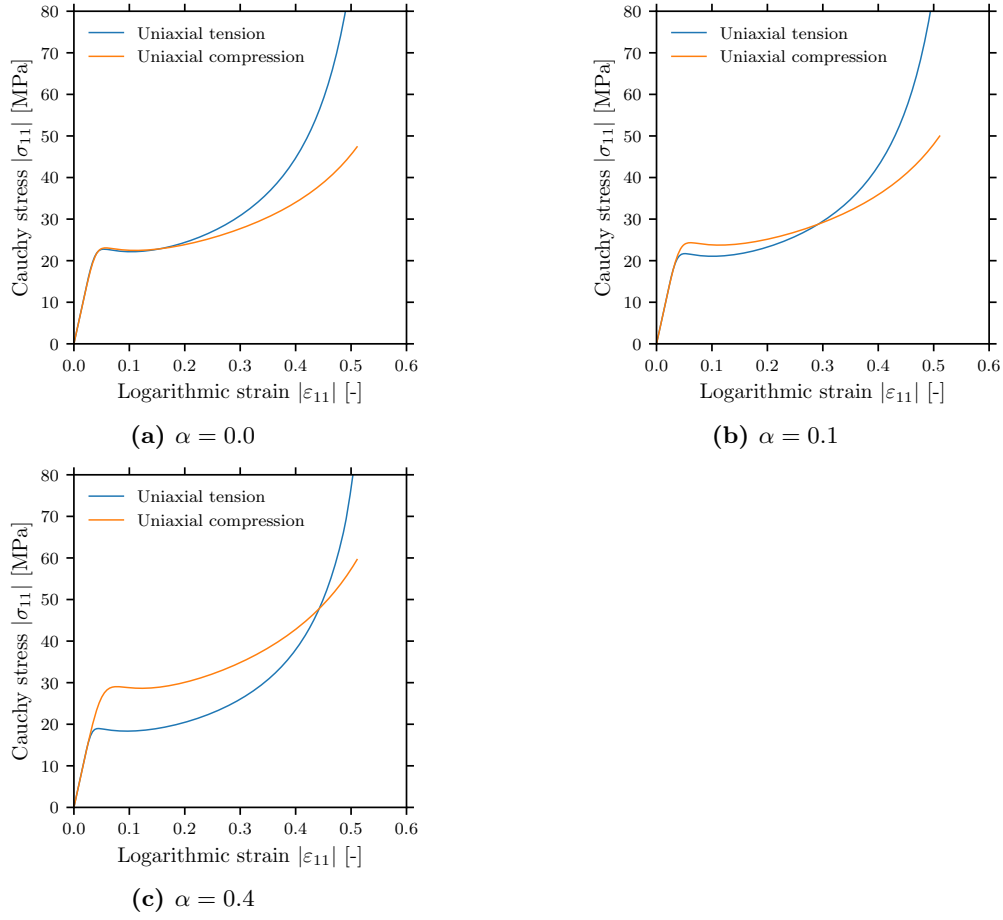
(a) $\alpha = 0.0$

(b) $\alpha = 0.1$

(c) $\alpha = 0.4$

Figure 9: Stress vs. strain curves comparing uniaxial tension and uniaxial compression single element simulations for different values of the parameter α. All analyses were performed with a nominal strain rate of $10^{-2} \, \mathrm{s}^{-1}$.

References

[1] E. M. Arruda and M. C. Boyce. 'A three-dimensional constitutive model for the large stretch behavior of rubber elastic materials'. In: *Journal of the Mechanics and Physics of Solids* 41.2 (1993), pp. 389–412. DOI: `10.1016/0022-5096(93)90013-6`.

[2] M. C. Boyce, G. G. Weber and D. M. Parks. 'On the kinematics of finite strain plasticity'. In: *Journal of the Mechanics and Physics of Solids* 37.5 (1989), pp. 647–665. DOI: `10.1016/0022-5096(89)90033-1`.

[3] M. E. Gurtin and L. Anand. 'The decomposition F = FeFp, material symmetry, and plastic irrotationality for solids that are isotropic-viscoplastic or amorphous'. In: *International Journal of Plasticity* 21.9 (2005), pp. 1686–1719. DOI: `10.1016/j.ijplas.2004.11.007`.

[4] J. S. Bergström and M. C. Boyce. 'Constitutive modeling of the large strain time-dependent behavior of elastomers'. In: *Journal of the Mechanics and Physics of Solids* 46.5 (1998), pp. 931–954. DOI: 10.1016/S0022-5096(97)00075-6.

[5] M. C. Boyce, D. M. Parks and A. S. Argon. 'Large inelastic deformation of glassy polymers. Part I: rate dependent constitutive model'. In: *Mechanics of materials* 7.1 (1988), pp. 15–33. DOI: https://doi.org/10.1016/0167-6636(88)90003-8.

[6] P. H. Holmström, A. H. Clausen, T. Berstad, D. Morin and O. S. Hopperstad. 'A pragmatic orthotropic elasticity-based damage model with spatially distributed properties applied to short glass-fibre reinforced polymers'. In: *International Journal of Solids and Structures* 230-231 (2021), p. 111142. DOI: 10.1016/J.IJSOLSTR.2021.111142.

[7] Z. P. Bažant and B. H. Oh. 'Crack band theory for fracture of concrete'. In: *Matériaux et Constructions* 16.3 (1983), pp. 155–177. DOI: 10.1007/BF02486267.

[8] O. Knoll. 'A Probabilistic Approach in Failure Modelling of Aluminium High Pressure Die-Castings'. PhD thesis. Department of Structural Engineering, NTNU, 2015.

[9] J. Johnsen, A. H. Clausen, F. Grytten, A. Benallal and O. S. Hopperstad. 'A thermo-elasto-viscoplastic constitutive model for polymers'. In: *Journal of the Mechanics and Physics of Solids* 124 (2019), pp. 681–701. DOI: https://doi.org/10.1016/j.jmps.2018.11.018.

[10] J. F. Berntsen. 'Testing and modelling of multimaterial joints'. PhD thesis. Department of Structural Engineering, NTNU, 2020.

[11] G. Marsaglia and T. A. Bray. 'A Convenient Method for Generating Normal Variables'. In: *http://dx.doi.org/10.1137/1006063* 6.3 (2006), pp. 260–264. DOI: 10.1137/1006063.